UDC 539.3: 624.195
IRSTI 30.19.15
REVIEW ARTICLE

IMPACT OF TRANSPORT LOAD ON A TUNNEL REINFORCED WITH A THREE-LAYER LINING

V. Ukrainets[1,*], Zh. Otarbaev[2], S. Girnis[1], L. Gorshkova[1], G. Murali[3]

[1]Toraighyrov University, 140008, Pavlodar, Kazakhstan
[2]National Engineering Academy of Kazakhstan, 050010, Almaty, Kazakhstan
[3]Graphic Era University, 248002, Dehradun, India

Abstract. *This paper presents an analytical solution to investigate the dynamic behavior of a shallow tunnel subjected to a stationary transport load (a load of constant form generated by uniformly moving traffic or transported cargo within the tunnel). The need to address this problem arises from the fact that the lining of the tunnel is still commonly analyzed using a highly simplified quasi-static method. The solution was based on mathematical modeling. The lining of the tunnel modeled in an elastic half-space consists of three rigidly connected cylindrical circular layers with different physical and mechanical properties: a thick middle layer (filler) and thin outer layers (facing). In the problem formulation, this lining is considered as a circular three-layer shell. The motion of the half-space and the middle layer of the shell is described by the exact equations of elasticity theory, while the motion of the thin inner shell layer (along which the load moves) and the thin outer layer is described by approximate equations. The case of a shallow tunnel reinforced with a three-layer steel-concrete lining (comprising a concrete filler and steel facing layers of equal thickness) subjected to a uniformly distributed axisymmetric normal load moving at a constant velocity within a specified interval is considered. Using the computer program developed by the authors based on the obtained analytical solution, numerical experiments were conducted to study the influence of the type of contact between the tunnel lining and the rock mass (rigid or sliding) on the stress-strain state of the lining and the rock mass.*

Keywords: *tunnel, elastic half-space, three-layer shell, moving load, displacements, stresses*

***Corresponding author**
Vitaliy Ukrainets, e-mail: vitnikukr@mail.ru

https://doi.org/10.51488/1680-080X/2025.4-26
Received 21 October 2025; Revised 12 December 2025; Accepted 25 January 2026

ӘОЖ 539.3: 624.195
ҒТАМР 30.19.15
ҒЫЛЫМИ МАҚАЛА

ТАЯЗ ОРНАЛАСҚАН ТОННЕЛЬДІҢ ҮШ ҚАБАТТЫ ҚАПТАМАСЫНА КӨЛІК ЖҮКТЕМЕСІНІҢ ӘСЕРІ

В. Украинец[1,*], Ж. Отарбаев[2], С. Гирнис[1], Л. Горшкова[1], Г. Мурали[3]

[1]Торайғыров университеті, 140008, Павлодар, Қазақстан
[2]ҚР Ұлттық инженерлік академиясы, 050010, Алматы, Қазақстан
[3]Graphic Era университеті, 248002, Дехрадун, Үндістан

Аңдатпа. *Бұл мақалада тоннель бойымен бірқалыпты қозғалатын көлік немесе тасымалданатын жүктен туындайтын тұрақты сипаттағы көлік жүктемесінің әсерінен таяз орналасқан тоннельдің динамикалық мінез-құлқын зерттеуге арналған есептің аналитикалық шешімі ұсынылған. Бұл мәселені қарастырудың қажеттілігі тоннель қаптамасын көлік жүктемесіне есептеу кезінде әлі күнге дейін айтарлықтай жуықталған квазистатикалық әдістің қолданылуымен түсіндіріледі. Шешім математикалық модельдеуге негізделген. Серпімді жартылай кеңістікте орналасқан тоннельдің қаптамасы әртүрлі физикалық-механикалық қасиеттерге ие үш өзара қатаң байланысқан цилиндрлік шеңберлі қабаттардан тұрады: қалың ортаңғы қабат (толтырғыш) және жұқа сыртқы қабаттар (қаптама). Есепті қою барысында бұл қаптама шеңберлі үш қабатты қабық ретінде қарастырылады. Жартылай кеңістіктің және қабықтың ортаңғы қабатының қозғалысы серпімділік теориясының дәл теңдеулерімен сипатталады, ал қабықтың ішкі жұқа қабатының (оның бойымен жүктеме қозғалады) және сыртқы жұқа қабатының қозғалысы жуықталған теңдеулермен сипатталады. Таяз орналасқан тоннельдің үш қабатты сталебетонды қаптамасына (бетон толтырғыштан және қалыңдықтары бірдей болат қаптама қабаттарынан тұратын) белгілі бір аралықта біркелкі таралған және тұрақты жылдамдықпен қозғалатын осьтік-симметриялық қалыпты жүктеменің әсері қарастырылған. Алынған аналитикалық шешім негізінде авторлар әзірлеген компьютерлік бағдарламаны пайдалана отырып, сандық эксперименттер жүргізілді. Зерттеу нәтижесінде тоннель қаптамасы мен жыныс массиві арасындағы байланыс түрінің (қатты немесе сырғымалы) олардың кернеулі-деформацияланған күйіне әсері талданды.*

Түйін сөздер: *тоннель, серпімді жартылай кеңістік, үш қабатты қабық, жылжымалы жүктеме, қозғалыстар, кернеулер*

***Автор-корреспондент**
Виталий Украинец, e-mail: vitnikukr@mail.ru

https://doi.org/10.51488/1680-080X/2025.4-26
Алынды 21 қазан 2025; Қайта қаралды 12 желтоқсан 2025; Қабылданды 25 қаңтар 2026

УДК 539.3: 624.195
МРНТИ 30.19.15
НАУЧНАЯ СТАТЬЯ

ВОЗДЕЙСТВИЕ ТРАНСПОРТНОЙ НАГРУЗКИ НА ПОДКРЕПЛЕННЫЙ ТРЕХСЛОЙНОЙ ОБДЕЛКОЙ ТОННЕЛЬ

В. Украинец[1]*, Ж. Отарбаев[2], С. Гирнис[1], Л. Горшкова[1], Г. Мурали[3]

[1]Торайгыров университет, 140008, Павлодар, Казахстан
[2]Национальная инженерная академия РК, 050010, Алматы, Казахстан
[3]Университет Graphic Era, 248002, Дехрадун, Индия

Аннотация. *В настоящей статье представлено аналитическое решение задачи для исследования динамического поведения тоннеля мелкого заложения при его нагружении стационарной транспортной нагрузкой (нагрузкой постоянного вида от равномерно движущегося по тоннелю транспорта или транспортируемого по нему груза). Необходимость решения данной задачи вызвана тем, что при расчете обделки тоннеля на транспортную нагрузку до сих пор используется весьма приближенный квазистатический метод. Решение основывалось на математическом моделировании. Обделка моделируемого в упругом полупространстве тоннеля состоит из трех жестко сопряженных между собой цилиндрических круговых слоев с разными физико-механическими свойствами: толстого среднего слоя (заполнителя) и тонких крайних слоев (обшивки). При постановке задачи эта обделка рассматривается как круговая трехслойная оболочка. Движение полупространства и среднего слоя оболочки описываются точными уравнениями теории упругости, движение тонкого внутреннего слоя оболочки (по которому движется нагрузка) и тонкого ее наружного слоя – приближенными уравнениями. Рассмотрен случай воздействия на трехслойную сталебетонную обделку (с бетонным заполнителем и стальной обшивкой со слоями одинаковой толщины) тоннеля мелкого заложения движущейся с постоянной скоростью осесимметричной нормальной нагрузки, равномерно распределенной в заданном интервале. При проведении, с использованием разработанной на основе полученного решения авторами компьютерной программы, численных экспериментов, исследовано влияние типа контакта обделки с породным массивом (жесткого и скользящего) на напряжённо-деформированное состояние обделки тоннеля и породного массива.*

Ключевые слова: *тоннель, упругое полупространство, трехслойная оболочка, движущаяся нагрузка, перемещения, напряжения*

***Автор-корреспондент**
Виталий Украинец, e-mail: vitnikukr@mail.ru

https://doi.org/10.51488/1680-080X/2025.4-26
Поступила 21 октября 2025; Пересмотрено 12 декабря 2025; Принято 25 января 2026

ACKNOWLEDGEMENTS/SOURCE OF FUNDING

The research was conducted using private sources of funding.

CONFLICT OF INTEREST

The authors state that there is no conflict of interest.

The authors declare that no generative artificial intelligence technologies or AI-based tools were used in the preparation of this article.

АЛҒЫС / ҚАРЖЫЛАНДЫРУ КӨЗІ

Зерттеу жеке қаржыландыру көздерін пайдалана отырып жүргізілді.

МҮДДЕЛЕР ҚАҚТЫҒЫСЫ

Авторлар мүдделер қақтығысы жоқ деп мәлімдейді.

Авторлар мақаланы дайындау барысында генеративті жасанды интеллект технологиялары мен жасанды интеллектке негізделген технологияларды пайдаланбағанын мәлімдейді.

БЛАГОДАРНОСТИ/ИСТОЧНИК ФИНАНСИРОВАНИЯ

Исследование проводилось с использованием частных источников финансирования.

КОНФЛИКТ ИНТЕРЕСОВ

Авторы заявляют, что конфликта интересов нет.

Авторы заявляют о том, что при подготовке статьи не использовались технологии генеративного искусственного интеллекта и технологии, основанные на искусственном интеллекте.

1 INTRODUCTION

The impact of transport loads in the tunnel causes vibrations in both the tunnel lining and the surrounding rock mass. Studies of these vibration processes by experimental methods require significant material costs, and in some cases, their implementation is not possible. Therefore, analytical and numerical research methods are needed. It should be noted that the deformations and stresses occurring in this structure are significantly dependent on the type and parameters of the transport load, the design of the tunnel lining, and the depth of its placement **(Sheng, 2019)**.

At present, the quasi-static method is still allowed in the analysis of tunnel lining under transport loads, using a highly simplified computational model – the "beam on elastic foundation". In this case, the dynamic effect of the transport load on the tunnel is taken into account using a dynamic amplification factor. For train speeds up to 70 km/h, the factor is recommended to be taken as 1.0, and for speeds of 70 km/h or higher – 1.1 **(SP 120.13330.2022)**. In this paper, the authors reject the use of such a model, which fails to reflect real conditions, and instead propose a dynamic method for analyzing a three-layer tunnel lining and the surrounding ground mass in shallow-buried tunnels, based on mathematical modeling. The computational model of the tunnel is a long circular three-layer shell embedded in an elastic half-space. The motion of the half-space and the middle layer of the shell is described by the exact equations of elasticity theory, while the motion of the thin inner shell layer (along which the load moves) and the thin outer layer is described by approximate equations.

It should be noted that the analytical solution presented in this paper for the model problem of determining the stress–strain state (SSS) of a three-layer tunnel lining in a shallow-buried tunnel and the surrounding rock mass is significantly more complex than the corresponding solution for a deep-buried tunnel reinforced with the same lining **(Alekseeva & Girnis, 2009, Otarbaev, 2018)**. In the latter case, the waves reflected from the ground surface, which arise due to the action of transport loads on the tunnel lining, can be neglected. Using a computer program developed by the authors based on the obtained analytical solution, numerical experiments were conducted to investigate the influence of the type of contact between the tunnel lining and the surrounding rock mass (rigid or sliding) on the stress–strain state of both the lining and the rock mass.

The reliability of the results is ensured by the correct formulation of the problem, the application of exact mathematical methods of elasticity theory in its solution, the rigor of the employed mathematical framework, the high degree of boundary condition satisfaction, and the agreement of the numerical results obtained in this work with certain previously published results by other authors.

The scientific contribution of this research consists in the development of a mathematically rigorous and physically adequate model of the dynamic behavior of a shallow-buried tunnel subjected to stationary transport loading, as well as in the implementation of computational tools based on this model. These tools enable the selection of optimal geometric and physico-mechanical characteristics of the tunnel structure during the design phase, taking into account the geotechnical conditions and loading parameters. Furthermore, the model facilitates prediction of the structure's performance during operation and the prevention of resonance phenomena that could lead to structural damage.

The main model problems for evaluating tunnel dynamics under stationary transport loading involve analyzing the behavior of a long circular cylindrical shell embedded either in an infinite elastic medium (corresponding to deep tunnels) or in a half-space (corresponding to shallow tunnels), subjected to a load moving along the shell's axis on its inner surface.

The model transport problem for a deep tunnel reinforced with a circular homogeneous lining has been studied by many researchers. Numerical methods such as the Finite Element Method (FE) **(Zhou et al., 2018)**, the coupled Finite Element Boundary Element Method (FE-BE) **(Sheng et al., 2005)**, and the Finite Difference Method (FD) have been used to study the problem of modeling ground vibrations caused by moving trains. These methods can simulate complex engineering envi-

ronments, but they require significant computational resources and data storage, which limits their practical application.

Analytical methods are more preferable for research in this field due to their computational efficiency.

In 2006, Forrest and Hunt **(Forrest & Hunt, 2006)** proposed the PiP model, in which the tunnel lining and the surrounding mass were modeled as a thin-walled circular shell and an infinitely thick pipe, respectively. A normal load is applied to the inner surface of the shell, which is rigidly bonded to the ground, acting at its lowest point and moving along the axis of the shell. The shell's movement is described by thin-walled shell theory equations, while the soil movement is described by elastic medium wave equations. Following **(Forrest & Hunt, 2006)**, Hussein and Hunt **(Hussein & Hunt, 2007)** modified the PiP model in 2007 to account for the case of an asymmetrical moving load on the shell. In 2014, Zeng **(Zeng et al., 2014)** further developed the model by representing the surrounding soil as a saturated poroelastic medium using Biot's theory.

In 2009, Gupta **(Gupta et al., 2009)** compared the periodic FE-BE model and the PiP model, examining the influence of lining and soil parameters on the dynamic behavior of tunnels. He demonstrated that material damping and the shear modulus of the soil have an important influence on the propagation of vibrations. The influence of structural changes to the tunnel, as well as geometrical properties such as the size and shape of the tunnel, is investigated. Additionally, it is demonstrated that the tunnel geometry has a considerable influence on the response closer to the tunnel.

In 2017, Dwivedi **(Dwivedi et al., 2017)** investigated the steady-state dynamic response of an infinitely long, elastic, homogeneous hollow cylinder of arbitrary thickness, imperfectly bonded to surrounding viscoelastic soil, under the action of a moving axisymmetric axial ring load. The soil was described using the Kelvin-Voigt model. The problem was solved using the Laplace transformation.

A more recent analytical approach to investigating the dynamic behavior of tunnels with homogeneous lining in layered soils was presented in **(Di et al., 2022)**, utilizing the method of separation of variables for the tunnel and the Helmholtz decomposition for the surrounding ground.

In the case of a tunnel lining consisting of different concentric layers, it is modeled as a layered circular cylindrical shell embedded in an elastic medium. Several studies **(Alekseeva & Girnis, 2009, Otarbaev, 2018, Otarbaev, 2015, Girnis & Bulyga, 2023)** have investigated the SSS of various configurations of layered shells, including three-layer shells with a thick middle layer and thin outer layers **(Alekseeva & Girnis, 2009, Otarbaev, 2018)** and two-layer shells **(Otarbaev, 2015, Girnis & Bulyga, 2023)**. These works also investigated the dynamic interaction with the surrounding medium and assessed the influence of critical load velocities.

For shallow tunnels, the solution of the transport problem becomes significantly more complex; therefore, the number of published studies in this area is limited.

To predict ground-borne vibrations from underground railway traffic, Degrande et al. **(Degrande et al., 2006)** developed a numerical periodic FE-BE method that accounts for the periodicity of the track structure. Yang and Hung **(Yang & Hung, 2008)** proposed a finite/infinite element method for analysing wave propagation problems caused by underground trains. The near field of the half-space, including the tunnel and parts of the soil, is simulated by finite elements, and the far field extending to infinity by infinite elements. Yang et al. introduced the scaled boundary finite element method (SBFEM) based on non-uniform rational B-splines (NURBS) using the concept of isogeometric analysis (IGA) for soil vibration problems, which is more efficient than the traditional FE method. In **(Yang & Li, 2022)**, the two-and-a-half-dimensional (2.5-D) version of IGA was formulated and used for predicting soil vibration caused by moving trains. For the soil-tunnel system, the IGA was used for the bounded domain (to account for geometric irregularities), while the scaled boundary isogeometric analysis (SBIGA) was applied to the unbounded domain (to model radiation damping at infinity). Most numerical models require significant computational effort, making them suitable for scientific research but still too expensive for use as design tools.

In 2017, **(Zhou et al., 2017)** proposed a two-step procedure for predicting vibrations in a poroelastic half-space induced by an underground train. The first step involves using an improved PiP model (coupled with the train-track system) to calculate the dynamic response (displacements and stresses) at the tunnel lining-soil interface in a poroelastic full-space. The actual poroelastic half-space vibrations are then calculated using a 2.5-D boundary integral equation for saturated porous media along with Green's function for a poroelastic half-space.

Analytical solutions were obtained in **(Yuan et al., 2017, Coşkun & Dolmaseven, 2017)** for problems involving a shallow tunnel reinforced with a homogeneous lining subjected to a moving point load **(Yuan et al., 2017)** or a uniformly distributed normal load **(Coşkun & Dolmaseven, 2017)**. In the problem formulation, the rock mass surrounding the tunnel lining was modeled as a viscoelastic half-space in **(Yuan et al., 2017)**, and as an elastic half-space in **(Coşkun & Dolmaseven, 2017)**.

Articles **(Alekseeva & Ukrainets, 2009, Alekseeva & Ukrainets, 2020, Otarbaev, 2022, Gorshkova, 2023, Stanevich, 2023, Otarbaev, 2024)** present analytical solutions to problems involving various types of moving loads acting on a homogeneous shell embedded in an elastic half-space and describe the results of numerical experiments conducted based on these solutions.

At present, three-layer tunnel linings – consisting of a thick intermediate layer (core material) and thin outer layers (facings) – have become widely used. Under bending conditions, three-layer shell structures are considered the most efficient, i.e., nearly optimal in terms of achieving minimal weight while satisfying given strength and stiffness constraints. Accordingly, a shallow tunnel lining of this type is investigated in the present study.

2 MATERIALS AND METHODS

The construction of the analytical solution to the problem formulated in this paper is based on mathematical modeling. To model the dynamic processes associated with wave propagation and diffraction in the tunnel lining and the surrounding rock mass under stationary transport loading, the following are employed: models of elastic media, thin and thick elastic shells, classical methods of partial variable separation and integral transforms, numerical methods for integration and for solving systems of algebraic equations, as well as the method of successive approximations **(Alekseeva & Ukrainets, 2009, Alekseeva & Ukrainets, 2020)**.

3 RESULTS AND DISCUSSION

As the computational model of the tunnel, we adopt the schematic representation of the tunnel shown in Cartesian (x, y, z) and cylindrical (r, θ, z) coordinates in **Figure 1**. In this model, the tunnel lining embedded in an elastic half-space is represented as a circular three-layer shell, with its z-axis parallel to the boundary of the half-space (the ground surface).

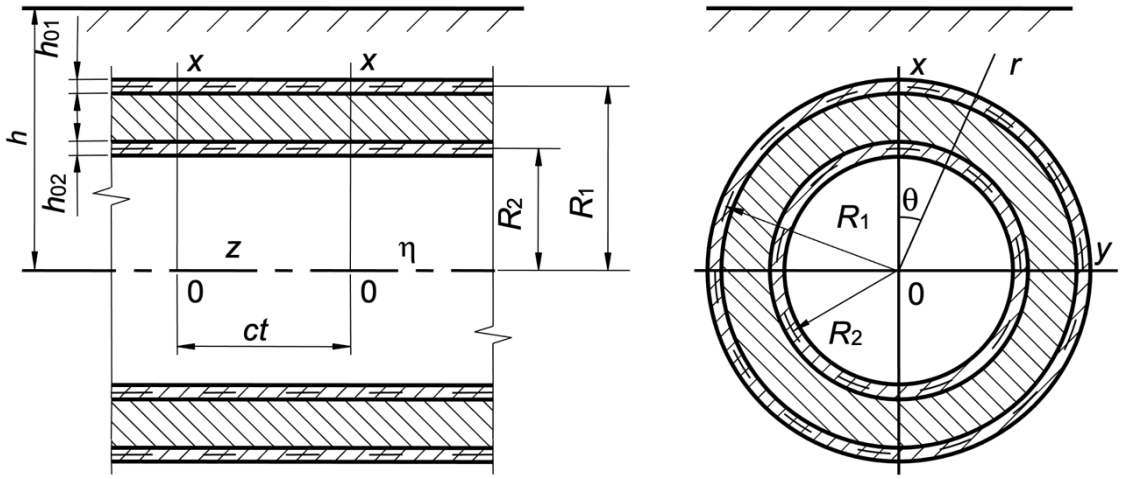

Figure 1 – Schematic representation of a tunnel at an embedment depth *h* (author's material)

The notation adopted in this study is as follows. For the half-space ($k=1$) and the middle layer (filler) of the shell оболочки ($k=2$): ν_k, μ_k, ρ_k denote the Poisson's ratio, shear modulus, and density, respectively; $c_{sk}=\sqrt{\mu_k/\rho_k}$ and $c_{pk}=\sqrt{(\lambda_k+2\mu_k)/\rho_k}$ represent the shear and longitudinal wave velocities, $\lambda_k=2\mu_k\nu_k/(1-2\nu_k)$. For the outer ($k=1$) and inner ($k=2$) thin-walled layers of the shell (the shell facing), which are rigidly bonded to the filler: $\nu_{0k}, \mu_{0k}, \rho_{0k}$ denote Poisson's ratio, shear modulus, and density, respectively; R_k is the radius of the mid-surface, and h_{0k} is the thickness. It is assumed that the shell facing is in contact with both the filler and the half-space at $r=R_k$.

The SSS of the half-space and the shell is determined under the action of a steady-state load of intensity P. Assuming that the load moves at a subcritical velocity $c<c_{sk}$, and switching to the moving coordinate systems ($x, y, \eta=z-ct$, $r, \theta, \eta=z-ct$), the motion of the half-space ($k=1$) and the filler of the shell ($k=2$) is described by Eqs. (1) **(Alekseeva & Girnis, 2009, Otarbaev, 2018, Otarbaev, 2015, Girnis & Bulyga, 2023, Alekseeva & Ukrainets, 2020)**, while the motion of the outer ($k=1$) and inner ($k=2$) thin-walled shell layers is described by Eqs. (2) **(Alekseeva & Girnis, 2009, Otarbaev, 2018)**.

$$\left(M_{pk}^{-2}-M_{sk}^{-2}\right)\operatorname{grad}\operatorname{div}\mathbf{u}_k+M_{sk}^{-2}\nabla^2\mathbf{u}_k=\partial^2\mathbf{u}_k/\partial\eta^2,\ k=1,2; \tag{1}$$

$$\begin{gathered}
\left[1-\frac{(1-\nu_{0k})\rho_{0k}c^2}{2\mu_{0k}}\right]\frac{\partial^2 u_{0\eta k}}{\partial\eta^2}+\frac{1-\nu_{0k}}{2R_k^2}\frac{\partial^2 u_{0\eta k}}{\partial\theta^2}+\frac{1+\nu_{0k}}{2R_k}\frac{\partial^2 u_{0\theta k}}{\partial\eta\partial\theta}+\frac{\nu_{0k}}{R_k}\frac{\partial u_{0rk}}{\partial\eta}=\frac{1-\nu_{0k}}{2\mu_{0k}h_{0k}}\left(q_{\eta k}-q_{\eta R_k}\right),\\
\frac{1+\nu_{0k}}{2R_k}\frac{\partial^2 u_{0\eta k}}{\partial\eta\partial\theta}+\frac{(1-\nu_{0k})}{2}\left(1-\frac{\rho_{0k}c^2}{\mu_{0k}}\right)\frac{\partial^2 u_{0\theta k}}{\partial\eta^2}+\frac{1}{R_k^2}\frac{\partial^2 u_{0\theta k}}{\partial\theta^2}+\frac{1}{R_k^2}\frac{\partial u_{0rk}}{\partial\theta}=\frac{1-\nu_{0k}}{2\mu_{0k}h_{0k}}\left(q_{\theta k}-q_{\theta R_k}\right),\\
\frac{\nu_{0k}}{R_k}\frac{\partial u_{0\eta k}}{\partial\eta}+\frac{1}{R_k^2}\frac{\partial u_{0\theta k}}{\partial\theta}+\frac{h_{0k}^2}{12}\nabla^2\nabla^2 u_{0rk}+\frac{(1-\nu_{0k})\rho_{0k}c^2}{2\mu_{0k}}\frac{\partial^2 u_{0rk}}{\partial\eta^2}+\frac{u_{0rk}}{R_k^2}=-\frac{1-\nu_{0k}}{2\mu_{0k}h_{0k}}\left(q_{rk}-q_{rR_k}\right).
\end{gathered} \tag{2}$$

Here $M_{sk}=c/c_{sk}$, $M_{pk}=c/c_{pk}$, ∇^2 – Laplace operator, $\mathbf{u}_k$ – displacement vectors of the points in the half-space and the core layer of the shell; $u_{0\eta k}$, $u_{0\theta k}$, u_{0rk} – displacements of points in the thin-walled layers of the shell; $q_{j1}=\sigma_{rj2}\big|_{r=R_1}$, $q_{jR_1}=\sigma_{rj1}\big|_{r=R_1}$, $q_{jR_2}=\sigma_{rj2}\big|_{r=R_2}$ – reactions of the

half-space and the filler (σ_{rj1}, σ_{rj2} – stresses in the half-space and the filler); $q_{j2} = P_j(\theta,\eta)$ ($P_j(\theta,\eta)$ – components of the $P(\theta,\eta)$); j = η, θ, r. When the shell is in sliding contact with the surrounding medium $q_{\eta R_1} = q_{\theta R_1} = 0$.

Vectors $\mathbf{u}_k$ can be represented through Lame potentials через потенциалы Ламе φ_{jk} (j = 1, 2, 3, k = 1, 2) **(Alekseeva & Girnis, 2009, Otarbaev, 2018, Otarbaev, 2015, Girnis & Bulyga, 2023, Alekseeva & Ukrainets, 2020)**

$$\mathbf{u}_k = \operatorname{grad}\varphi_{1k} + \operatorname{rot}\left(\varphi_{2k}\mathbf{e}_\eta\right) + \operatorname{rot}\operatorname{rot}\left(\varphi_{3k}\mathbf{e}_\eta\right),\ \ k = 1, 2, \tag{3}$$

where e_η – denotes the unit vector along the axis η.
From (1) and (3) it follows:

$$\nabla^2\varphi_{jk} = M_{jk}^2\,\partial^2\varphi_{jk}\big/\partial\eta^2,\ j = 1, 2, 3,\ \ k = 1, 2, \tag{4}$$

where $M_{1k} = M_{pk}$, $M_{2k} = M_{3k} = M_{sk}$.
From (3) it follows (for k = 1, 2)

$$\begin{aligned} u_{rk} &= \frac{\partial\varphi_{1k}}{\partial r} + \frac{1}{r}\frac{\partial\varphi_{2k}}{\partial\theta} + \frac{\partial^2\varphi_{3k}}{\partial\eta\partial r}, \\ u_{\theta k} &= \frac{1}{r}\frac{\partial\varphi_{1k}}{\partial\theta} - \frac{\partial\varphi_{2k}}{\partial r} + \frac{1}{r}\frac{\partial^2\varphi_{3k}}{\partial\eta\partial\theta}, \\ u_{\eta k} &= \frac{\partial\varphi_{1k}}{\partial\eta} + m_{sk}^2\frac{\partial^2\varphi_{3k}}{\partial\eta^2}; \end{aligned} \tag{5}$$

$$\begin{aligned} u_{x1} &= \frac{\partial\varphi_{11}}{\partial x} + \frac{\partial\varphi_{21}}{\partial y} + \frac{\partial^2\varphi_{31}}{\partial x\partial\eta}, \\ u_{y1} &= \frac{\partial\varphi_{11}}{\partial y} - \frac{\partial\varphi_{21}}{\partial x} + \frac{\partial^2\varphi_{31}}{\partial y\partial\eta}, \\ u_{\eta 1} &= \frac{\partial\varphi_{11}}{\partial\eta} + m_{s1}^2\frac{\partial^2\varphi_{31}}{\partial\eta^2}. \end{aligned} \tag{6}$$

Here $m_{sk}^2 = 1 - M_{sk}^2 > 0$.
Using (5), (6), and Hooke's law, we obtain (for k = 1, 2)

$$\begin{aligned} \sigma_{\eta\eta k} &= (2\mu_k + \lambda_k M_{pk}^2)\frac{\partial^2\varphi_{1k}}{\partial\eta^2} + 2\mu_k m_{sk}^2\frac{\partial^3\varphi_{3k}}{\partial\eta^3}, \\ \sigma_{\theta\theta k} &= \lambda_k M_{pk}^2\frac{\partial^2\varphi_{1k}}{\partial\eta^2} + \frac{2\mu_k}{r}\left(\frac{1}{r}\frac{\partial^2\varphi_{1k}}{\partial\theta^2} + \frac{\partial\varphi_{1k}}{\partial r} + \frac{1}{r}\frac{\partial\varphi_{2k}}{\partial\theta} - \frac{\partial^2\varphi_{2k}}{\partial r\partial\theta} + \frac{1}{r}\frac{\partial^3\varphi_{3k}}{\partial\theta^2\partial\eta} + \frac{\partial^2\varphi_{3k}}{\partial r\partial\eta}\right), \\ \sigma_{rrk} &= \lambda_k M_{pk}^2\frac{\partial^2\varphi_{1k}}{\partial\eta^2} + 2\mu_k\left(\frac{\partial^2\varphi_{1k}}{\partial r^2} + \frac{1}{r}\frac{\partial^2\varphi_{2k}}{\partial\theta\partial r} - \frac{1}{r^2}\frac{\partial\varphi_{2k}}{\partial\theta} + \frac{\partial^3\varphi_{3k}}{\partial r^2\partial\eta}\right), \\ \sigma_{r\eta k} &= \mu_k\left(2\frac{\partial^2\varphi_{1k}}{\partial\eta\partial r} + \frac{1}{r}\frac{\partial^2\varphi_{2k}}{\partial\theta\partial\eta} + (1 + m_{sk}^2)\frac{\partial^3\varphi_{3k}}{\partial\eta^2\partial r}\right), \end{aligned} \tag{7}$$

$$\sigma_{\eta\theta k}=\mu_k\left(\frac{2}{r}\frac{\partial^2\varphi_{1k}}{\partial\theta\partial\eta}-\frac{\partial^2\varphi_{2k}}{\partial r\partial\eta}+\frac{(1+m_{sk}^2)}{r}\frac{\partial^3\varphi_{3k}}{\partial\theta\partial\eta^2}\right),$$

$$\sigma_{r\theta k}=2\mu_k\left(\frac{1}{r}\frac{\partial^2\varphi_{1k}}{\partial\theta\partial r}-\frac{1}{r^2}\frac{\partial\varphi_{1k}}{\partial\theta}-\frac{\partial^2\varphi_{2k}}{\partial r^2}-\frac{m_{sk}^2}{2}\frac{\partial^2\varphi_{2k}}{\partial\eta^2}+\frac{1}{r}\frac{\partial^3\varphi_{3k}}{\partial r\partial\eta\partial\theta}-\frac{1}{r^2}\frac{\partial^2\varphi_{3k}}{\partial\eta\partial\theta}\right);$$

$$\sigma_{\eta\eta 1}=(2\mu_1+\lambda_1M_{p1}^2)\frac{\partial^2\varphi_{11}}{\partial\eta^2}+2\mu_1m_{s1}^2\frac{\partial^3\varphi_{31}}{\partial\eta^3},$$

$$\sigma_{yy1}=\lambda_1M_{p1}^2\frac{\partial^2\varphi_{11}}{\partial\eta^2}+2\mu_1\left(\frac{\partial^2\varphi_{11}}{\partial y^2}-\frac{\partial^2\varphi_{21}}{\partial x\partial y}+\frac{\partial^3\varphi_{31}}{\partial y^2\partial\eta}\right),$$

$$\sigma_{xx1}=\lambda_1M_{p1}^2\frac{\partial^2\varphi_{11}}{\partial\eta^2}+2\mu_1\left(\frac{\partial^2\varphi_{11}}{\partial x^2}+\frac{\partial^2\varphi_{21}}{\partial x\partial y}+\frac{\partial^3\varphi_{31}}{\partial x^2\partial\eta}\right),$$

$$\sigma_{x\eta 1}=\mu_1\left(2\frac{\partial^2\varphi_{11}}{\partial\eta\partial x}+\frac{\partial^2\varphi_{21}}{\partial y\partial\eta}+(1+m_{s1}^2)\frac{\partial^3\varphi_{31}}{\partial\eta^2\partial x}\right), \tag{8}$$

$$\sigma_{\eta y1}=\mu_1\left(2\frac{\partial^2\varphi_{11}}{\partial y\partial\eta}-\frac{\partial^2\varphi_{21}}{\partial x\partial\eta}+(1+m_{s1}^2)\frac{\partial^3\varphi_{31}}{\partial y\partial\eta^2}\right),$$

$$\sigma_{xy1}=2\mu_1\left(\frac{\partial^2\varphi_{11}}{\partial x\partial y}-\frac{\partial^2\varphi_{21}}{\partial x^2}-\frac{m_{s1}^2}{2}\frac{\partial^2\varphi_{21}}{\partial\eta^2}+\frac{\partial^3\varphi_{31}}{\partial x\partial y\partial\eta}\right).$$

If no load is applied to the ground surface, then at $x = h$

$$\sigma_{xx1}=\sigma_{xy1}=\sigma_{x\eta 1}=0. \tag{9}$$

Depending on the contact conditions between the shell and the surrounding elastic medium, the following holds:

- in the case of sliding contact

$$\begin{aligned}&\text{at } r=R_1\ \ u_{r1}=u_{r2},\ u_{j2}=u_{0j1},\ \sigma_{r\eta 1}=0,\ \sigma_{r\theta 1}=0,\\&\text{at } r=R_2\ \ u_{j2}=u_{0j2},\quad j=r,\theta,\eta;\end{aligned} \tag{10}$$

- in the case of rigid contact

$$\begin{aligned}&\text{at } r=R_1\ \ u_{j1}=u_{j2},\ u_{j1}=u_{0j1},\\&\text{at } r=R_2\ \ u_{j2}=u_{0j2},\ j=r,\theta,\eta.\end{aligned} \tag{11}$$

The load moving along the shell is represented as

$$\begin{aligned}P(\theta,\eta)&=p(\theta)e^{i\xi\eta},\quad p(\theta)=\sum_{n=-\infty}^{\infty}P_ne^{in\theta},\\P_j(\theta,\eta)&=p_j(\theta)e^{i\xi\eta},\quad p_j(\theta)=\sum_{n=-\infty}^{\infty}P_{nj}e^{in\theta},\quad j=r,\theta,\eta.\end{aligned} \tag{12}$$

Given the steady-state nature of the process,

$$\varphi_{jk}(r,\theta,\eta)=\Phi_{jk}(r,\theta)e^{i\xi\eta},\ \ j=1,2,3,\ \ k=1,2; \tag{13}$$

$$u_{0jk}(\theta,\eta)=\sum_{n=-\infty}^{\infty}u_{0njk}e^{in\theta}e^{i\xi\eta},\ j=r,\theta,\eta,\ k=1,2\,. \tag{14}$$

Substituting (13) into (4) yields

$$\nabla_2^2\Phi_{jk}-m_{jk}^2\xi^2\Phi_{jk}=0,\ j=1,2,3,\ \ k=1,2\,. \tag{15}$$

Here $m_{jk}=\sqrt{1-M_{jk}^2}$, $m_{1k}=m_{pk}$, $m_{2k}=m_{3k}=m_{sk}$, ∇_2^2 – two-dimensional Laplace operator.

With the accepted speed limit $c < c_{sk}$ ($M_{sk} < 1$, $k = 1, 2$) solutions to Eqs. (15) can be represented in the form

$$\Phi_{jk}=\Phi_{jk}^{(1)}+\Phi_{jk}^{(2)},\ j=1,2,3,\ \ k=1,2\,, \tag{16}$$

where:

- for elastic medium

$$\Phi_{j1}^{(1)}=\sum_{n=-\infty}^{\infty}a_{nj}K_n(k_{j1}r)e^{in\theta}\,,\ \Phi_{j1}^{(2)}=\int_{-\infty}^{\infty}g_j(\xi,\zeta)\exp\left(iy\zeta+(x-h)\sqrt{\zeta^2+k_{j1}^2}\right)d\zeta\,;$$

- for shell filler

$$\Phi_{j2}^{(1)}=\sum_{n=-\infty}^{\infty}a_{nj+3}K_n(k_{j2}r)e^{in\theta}\,,\ \Phi_{j2}^{(2)}=\sum_{n=-\infty}^{\infty}a_{nj+6}I_n(k_{j2}r)\,e^{in\theta}\,.$$

Here $K_n(k_jr), I_n(k_jr)$ – respectively, Macdonald functions and modified Bessel functions, $k_{j1}=\left|m_{j1}\xi\right|$, $k_{j2}=\left|m_{j2}\xi\right|$; $a_{n1},...,a_{n9}$, $g_j(\xi,\zeta)$ – unknown coefficients and functions, $j = 1, 2, 3$.

In Cartesian coordinates, Φ_{j1} (16) take the form

$$\Phi_{j1}=\int_{-\infty}^{\infty}\left[\frac{e^{-xf_j}}{2f_j}\sum_{n=-\infty}^{\infty}a_{nj}\Phi_{nj}+g_j(\xi,\zeta)e^{(x-h)f_j}\right]e^{iy\zeta}d\zeta\,. \tag{17}$$

Here $\Phi_{nj}=\left[\left(\zeta+f_j\right)/k_{j1}\right]^n$, $f_j=\sqrt{\zeta^2+k_{j1}^2}$, $j=1,2,3$.

The boundary conditions (9) are applied, with reference to (8), (13), and (17). Equating the coefficients at $e^{iy\zeta}$ to zero yields a system of three algebraic equations, from which we determine

$$g_j(\xi,\zeta)=\frac{1}{\Delta_*}\sum_{l=1}^{3}\Delta_{jl}^*e^{-hf_l}\sum_{n=-\infty}^{\infty}a_{nl}\Phi_{nl}\,. \tag{18}$$

Here $\Delta_*=\left(2\rho_*^2-\beta^2\right)^2-4\rho_*^2\sqrt{\rho_*^2-\alpha^2}\sqrt{\rho_*^2-\beta^2}$,

$$\Delta_{11}^*=\frac{\Delta_*}{2\sqrt{\rho_*^2-\alpha^2}}-\frac{\left(2\rho_*^2-\beta^2\right)^2}{\sqrt{\rho_*^2-\alpha^2}},\ \Delta_{12}^*=-2\zeta\left(2\rho_*^2-\beta^2\right),\ \Delta_{13}^*=2\xi\left(2\rho_*^2-\beta^2\right)\sqrt{\rho_*^2-\beta^2},$$

$$\Delta_{21}^*=-\frac{M_{s1}^2}{m_{s1}^2}\Delta_{12}^*,\quad \Delta_{22}^*=-\frac{\Delta_{**}}{2\sqrt{\rho_*^2-\beta^2}},\quad \Delta_{23}^*=-4\xi\zeta\frac{M_{s1}^2}{m_{s1}^2}\sqrt{\rho_*^2-\alpha^2}\sqrt{\rho_*^2-\beta^2},$$

$$\Delta_{31}^{*}=-\frac{\Delta_{13}^{*}}{m_{s1}^{2}\xi^{2}},\quad \Delta_{32}^{*}=\frac{\Delta_{21}^{*}}{\beta^{2}},\quad \Delta_{33}^{*}=-\frac{\Delta_{**}}{2\sqrt{\rho_{*}^{2}-\beta^{2}}}+\frac{\left(2\rho_{*}^{2}-\beta^{2}\right)^{2}}{\sqrt{\rho_{*}^{2}-\beta^{2}}},$$

$$\Delta_{**}=\left(2\rho_{*}^{2}-\beta^{2}\right)^{2}-4\rho_{**}^{2}\sqrt{\rho_{*}^{2}-\alpha^{2}}\sqrt{\rho_{*}^{2}-\beta^{2}},$$

$$\alpha=M_{p1}\xi,\quad \beta=M_{s1}\xi,\quad \rho_{*}^{2}=\xi^{2}+\zeta^{2},\quad \rho_{**}^{2}=\xi^{2}+\left(2/m_{s1}^{2}-1\right)\zeta^{2}.$$

The investigation of the determinant $\Delta_{*}(\xi,\zeta)$ showed that $\Delta_{*}(\xi,\zeta)\neq 0$, when $c < c_R$ (where c_R is the Rayleigh surface wave velocity in the half-space).

Taking into account (18), expressions for potentials Φ_{j1} in the Cartesian coordinate system (17) for $c < c_R$ take the form

$$\Phi_{j1}=\int_{-\infty}^{\infty}\left[\frac{e^{-xf_j}}{2f_j}\sum_{n=-\infty}^{\infty}a_{nj}\Phi_{nj}+e^{(x-h)f_j}\sum_{l=1}^{3}\frac{\Delta_{jl}^{*}}{\Delta_{*}}e^{-hf_l}\sum_{n=-\infty}^{\infty}a_{nl}\Phi_{nl}\right]e^{iy\zeta}d\zeta.$$

Using the relation

$$\exp\left(iy\zeta+(x-h)\sqrt{\zeta^{2}+k_j^{2}}\right)=\sum_{n=-\infty}^{\infty}I_n(k_jr)e^{in\theta}\left[\left(\zeta+\sqrt{\zeta^{2}+k_j^{2}}\right)/k_j\right]^{n}e^{-h\sqrt{\zeta^{2}+k_j^{2}}},$$

we represent the potentials Φ_{j1} (16), taking into account (18), in a cylindrical coordinate system at $c < c_R$

$$\Phi_{j1}=\sum_{n=-\infty}^{\infty}\left(a_{nj}K_n(k_{j1}r)+b_{nj}I_n(k_{j1}r)\right)e^{in\theta}. \tag{19}$$

Here $b_{nj}=\sum_{l=1}^{3}\sum_{m=-\infty}^{\infty}a_{ml}A_{nj}^{ml}$, $A_{nj}^{ml}=\int_{-\infty}^{\infty}\frac{\Delta_{jl}^{*}}{\Delta_{*}}\Phi_{ml}\Phi_{nj}e^{-h(f_l+f_j)}d\zeta$.

Substituting expressions (13) into (5) and (7), taking into account (19), yields the formulas for calculating the displacements u_{l1}^{*} and stresses σ_{lm1}^{*} (l, m = r, θ, η) in the elastic medium for $c < c_R$ (* denotes that these displacements and stresses correspond to the case of a load acting on the shell, as defined in (12)). Similarly, substituting (16) for $k = 2$, taking into account (13), into (5) and (7), provides the formulas for calculating the displacements u_{l2}^{*} and stresses σ_{lm2}^{*} (l, m = r, θ, η) in the shell filler for $c < c_R$.

By substituting (14) into (2) and solving the resulting system of equations for the n-th term of the expansion with respect to $u_{0n\eta k}$, $u_{0n\theta k}$, u_{0nrk}, we can obtain the expressions for these variables, which are presented in **(Alekseeva & Girnis, 2009, Otarbaev, 2018)**.

Substituting the expression for the load (12) and the corresponding displacement and stress expressions into the boundary conditions (10) or (11), and then equating the coefficients of the series in terms of $e^{in\theta}$, we obtain an infinite system of $n=0,\pm1,\pm2,...$ linear algebraic equations, from which the coefficients $a_{n1},...,a_{n9}$ are determined. When solving this system using the method of successive approximations **(Alekseeva & Ukrainets, 2009)**, each successive approximation involves solving a system of linear algebraic equations of block-diagonal form with 9×9 matrices and determinants $\Delta_n(\xi,c)$ along the main diagonal.

If a load of type $P(\theta,\eta)=p(\theta)p(\eta)$ moves along the shell, then by representing this load, as well as the components of the SSS of the half-space and the shell filler, in the form of Fourier integrals, we obtain

$$P(\theta,\eta)=\frac{1}{2\pi}\int_{-\infty}^{\infty}P^{*}(\theta,\xi)e^{i\xi\eta}d\xi=p(\theta)p(\eta)=p(\theta)\frac{1}{2\pi}\int_{-\infty}^{\infty}p^{*}(\xi)e^{i\xi\eta}d\xi,$$

$$P_m(\theta,\eta)=\frac{1}{2\pi}\int_{-\infty}^{\infty}P_m^*(\theta,\xi)e^{i\xi\eta}d\xi=p_m(\theta)p(\eta)=p_m(\theta)\frac{1}{2\pi}\int_{-\infty}^{\infty}p^*(\xi)e^{i\xi\eta}d\xi;$$

$$u_{lk}(r,\theta,\eta)=\frac{1}{2\pi}\int_{-\infty}^{\infty}u_{lk}^*(r,\theta,\xi)p^*(\xi)d\xi,$$
$$\sigma_{lmk}(r,\theta,\eta)=\frac{1}{2\pi}\int_{-\infty}^{\infty}\sigma_{lmk}^*(r,\theta,\xi)p^*(\xi)d\xi. \quad (20)$$

Here $l=r,\theta,\eta,\ m=r,\theta,\eta,\ k=1,2;\ p^*(\xi)=\int_{-\infty}^{\infty}p(\eta)e^{-i\xi\eta}d\eta$.

If $\Delta_n(\xi,c)\neq 0$, then any numerical integration method can be used for computing (20). Numerical investigations of $\Delta_n(\xi, c)$ have shown that these determinants are nonzero when $c < c_{(n)*}$. Here $c_{(n)*}$ are the critical load velocities, which may be lower than c_R. As follows from the calculations, $\min c_{(n)*} = c_{(0)*}$ **(Alekseeva & Girnis, 2009, Girnis & Bulyga, 2023, Alekseeva & Ukrainets, 2009)**.

Consider a tunnel with a depth of h = 6 m in a rock mass with physical and mechanical characteristics: $\nu_1 = 0.294$, $\mu_1 = \mu = 1.09\cdot10^8$ Pa, $\rho_1 = 1.5\cdot10^3$ kg/m^3. The tunnel is reinforced with a three-layer steel-concrete lining. The contact between the lining layers is rigid. The lining consists of two thin-walled steel ($\nu_{01} = \nu_{02} = 0.3$, $\mu_{01} = \mu_{02} = 8.08\cdot10^{10}$ Pa, $\rho_{01} = \rho_{02} = 7.8\cdot10^3$ kg/m^3) shells ($h_{01} = h_{02} = 0{,}02$ m; $R_1 = 3.0$ m, $R_2 = 2.5$ m). The filler material between the shells is concrete ($\nu_2 = 0{,}2$, $\mu_2 = 1.21\cdot10^{10}$ Pa, $\rho_2 = 2.5\cdot10^3$ kg/m$\cdot10^3$). It should be noted that the stiffness of the lining materials exceeds that of the material composing the surrounding rock mass.

An axisymmetric normal load with intensity Q (Pa) moves through the tunnel at a speed of c = 100 m/s. The load applies uniform pressure to the tunnel lining within the interval $|\eta| \le l_0 = 0.2$ m. The intensity Q is chosen such that the total load over the loading section of length $2l_0$ is equal to the intensity of an equivalent concentrated normal ring load $P^{\circ\circ}$ (N/m), i.e. $Q = P^{\circ\circ}/2l_0$.

The following notation is adopted with indices k = 1, 2 in the components of displacements and stresses omitted for brevity: $u_r^\circ = u_r\mu/P^\circ$ (m), $\sigma_{rr}^\circ = \sigma_{rr}/P^\circ$, $\sigma_{\theta\theta}^\circ = \sigma_{\theta\theta}/P^\circ$, $\sigma_{\eta\eta}^\circ = \sigma_{\eta\eta}/P^\circ$, $u_x^\circ = u_x\mu/P^\circ$ (m), $u_y^\circ = u_y\mu/P^\circ$ (m), $\sigma_{yy}^\circ = \sigma_{yy}/P^\circ$, where $P^\circ = P^{\circ\circ}/\text{m}$ (Pa).

The results of the SSS calculations for the tunnel lining filler and the surrounding rock mass in the xy plane are presented in Tables 1 – 3. Table 1 presents the values of the SSS components on the inner ($r = R_2$) and outer ($r = R_1$) surfaces of the tunnel lining filler. Table 2 contains the SSS components at the contact surface ($r = R_1$) of the rock mass. Table 3 provides the SSS components of the ground surface ($x = h$), which were used to construct the plots shown in **Figures 2 – 5**. Curves 1 correspond to rigid contact of the lining with the rock mass, and curves 2 to sliding contact.

Table 1
Stress-strain components at the tunnel lining filler in the xy plane (author's material)

r	SSS components	|θ|, degree									
		0	**20**	**40**	**60**	**80**	**100**	**120**	**140**	**160**	**180**
Rigid contact between the lining and the rock mass											
R_2	$u^{\circ}_r\times10$	0.19	0.19	0.19	0.18	0.18	0.18	0.18	0.18	0.18	0.18
	σ°_{rr}	-2.4	-2.4	-2.4	-2.4	-2.4	-2.4	-2.4	-2.4	-2.4	-2.4
	$\sigma^{\circ}_{\theta\theta}$	0.93	0.93	0.93	0.93	0.93	0.93	0.92	0.92	0.92	0.92
	$\sigma^{\circ}_{\eta\eta}$	-2.37	-2.37	-2.37	-2.37	-2.37	-2.38	-2.38	-2.38	-2.38	-2.38
R_1	$u^{\circ}_r\times10$	0.16	0.16	0.16	0.16	0.15	0.15	0.15	0.15	0.15	0.15
	σ°_{rr}	-0.12	-0.12	-0.12	-0.12	-0.12	-0.12	-0.12	-0.12	-0.12	-0.12
	$\sigma^{\circ}_{\theta\theta}$	1.61	1.61	1.60	1.60	1.60	1.60	1.60	1.60	1.60	1.60
	$\sigma^{\circ}_{\eta\eta}$	1.29	1.28	1.28	1.28	1.27	1.27	1.27	1.27	1.27	1.27
Sliding contact between the lining and the rock mass											
R_2	$u^{\circ}_r\times10$	0.19	0.19	0.19	0.19	0.18	0.18	0.18	0.18	0.18	0.18
	σ°_{rr}	-2.4	-2.4	-2.4	-2.4	-2.4	-2.4	-2.4	-2.4	-2.4	-2.4
	$\sigma^{\circ}_{\theta\theta}$	0.94	0.94	0.94	0.94	0.94	0.94	0.94	0.94	0.93	0.93
	$\sigma^{\circ}_{\eta\eta}$	-2.38	-2.38	-2.38	-2.38	-2.38	-2.38	-2.38	-2.38	-2.38	-2.38
R_1	$u^{\circ}_r\times10$	0.16	0.16	0.16	0.16	0.16	0.15	0.15	0.15	0.15	0.15
	σ°_{rr}	-0.12	-0.12	-0.12	-0.12	-0.12	-0.12	-0.12	-0.12	-0.12	-0.12
	$\sigma^{\circ}_{\theta\theta}$	1.63	1.63	1.62	1.62	1.61	1.61	1.61	1.62	1.62	1.62
	$\sigma^{\circ}_{\eta\eta}$	1.32	1.32	1.31	1.31	1.30	1.30	1.30	1.30	1.30	1.30

Table 2
Stress-strain components at the contact surface ($r = R_1$) of the rock mass in the xy plane (author's material)

SSS components	|θ|, degree									
	0	**20**	**40**	**60**	**80**	**100**	**120**	**140**	**160**	**180**
Rigid contact between the lining and the rock mass										
$u^{\circ}_r\times10$	0.16	0.16	0.16	0.16	0.15	0.15	0.15	0.15	0.15	0.15
$\sigma^{\circ}_{rr}\times10$	-0.32	-0.32	-0.33	-0.34	-0.34	-0.34	-0.34	-0.34	-0.34	-0.34
$\sigma^{\circ}_{\theta\theta}\times10$	0.05	0.04	0.04	0.04	0.04	0.04	0.03	0.03	0.03	0.03
$\sigma^{\circ}_{\eta\eta}\times10$	0.02	0.01	0.01	0.01	0.01	0.01	0.0	0.0	0.0	0.0
Sliding contact between the lining and the rock mass										
$u^{\circ}_r\times10$	0.16	0.16	0.16	0.16	0.16	0.15	0.15	0.15	0.15	0.15
$\sigma^{\circ}_{rr}\times10$	-0.25	-0.26	-0.28	-0.29	-0.29	-0.29	-0.29	-0.29	-0.29	-0.29
$\sigma^{\circ}_{\theta\theta}\times10$	-0.03	-0.03	-0.02	-0.02	-0.02	-0.02	-0.03	-0.03	-0.03	-0.03
$\sigma^{\circ}_{\eta\eta}\times10$	-0.26	-0.26	-0.26	-0.26	-0.26	-0.26	-0.26	-0.26	-0.26	-0.26

Table 3
Stress-strain components at the Earth's surface ($x = h$) in the xy plane

SSS components	*y*, m								
	0.0	**0.4**	**0.8**	**1.2**	**1.6**	**2.0**	**2.4**	**2.8**	**3.2**
Rigid contact between the lining and the rock mass									
$u^{\circ}_x \times 100$	0.56	0.56	0.55	0.53	0.51	0.49	0.46	0.44	0.41
$u^{\circ}_y \times 100$	0.0	0.03	0.05	0.09	0.09	0.10	0.11	0.11	0.10
$\sigma^{\circ}_{yy} \times 100$	0.34	0.33	0.31	0.28	0.24	0.19	0.15	0.11	0.08
$\sigma^{\circ}_{\eta\eta} \times 100$	0.55	0.55	0.54	0.51	0.48	0.45	0.42	0.38	0.35
Sliding contact between the lining and the rock mass									
$u^{\circ}_x \times 100$	0.68	0.68	0.67	0.65	0.62	0.59	0.56	0.53	0.50
$u^{\circ}_y \times 100$	0.0	0.03	0.06	0.09	0.11	0.12	0.13	0.13	0.13
$\sigma^{\circ}_{yy} \times 100$	0.41	0.40	0.37	0.34	0.29	0.24	0.19	0.14	0.09
$\sigma^{\circ}_{\eta\eta} \times 100$	0.68	0.67	0.65	0.62	0.59	0.55	0.51	0.47	0.44

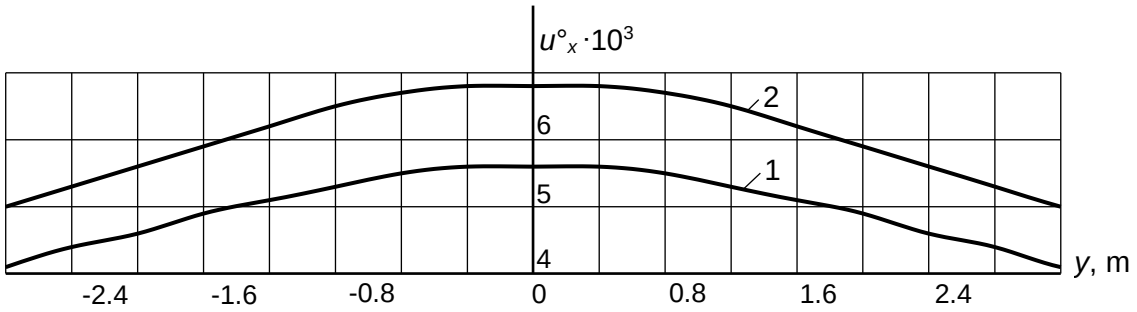

Figure 2 – Displacement components u°_x at the Earth's surface in the xy plane (author's material)

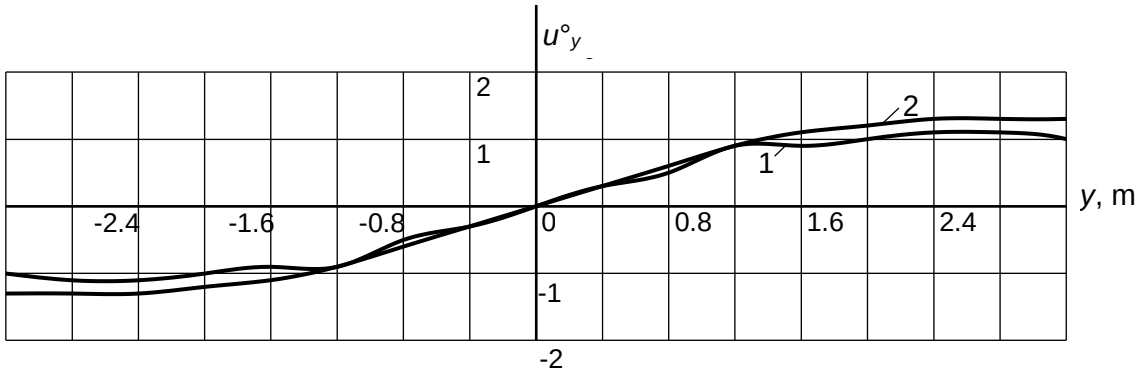

Figure 3 – Displacement components u°_y at the Earth's surface in the xy plane (author's material)

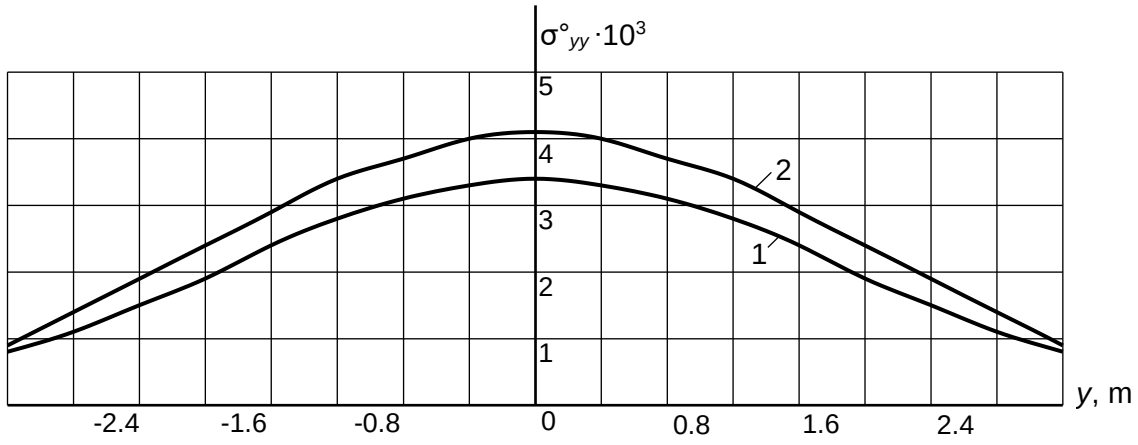

Figure 4 – Stress components σ°_{yy} at the Earth's surface in the xy plane (author's material)

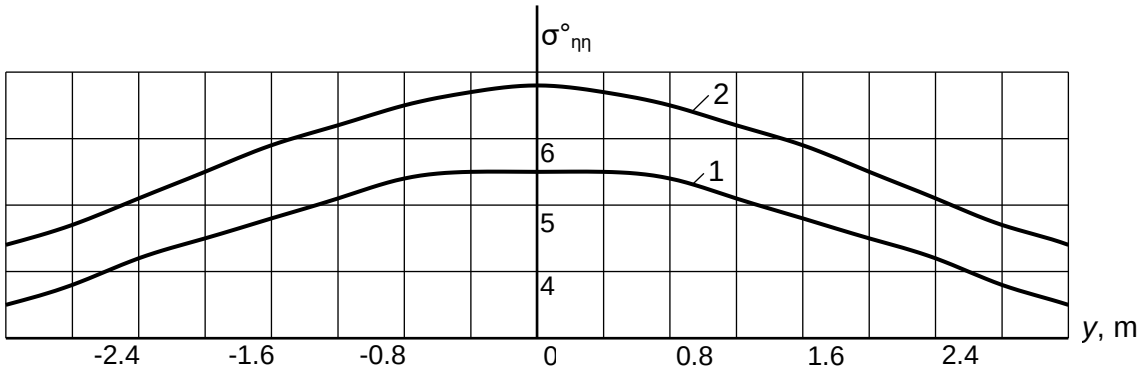

Figure 5 – Stress components $\sigma^{\circ}_{\eta\eta}$ at the Earth's surface in the xy plane (author's material)

The obtained results are analyzed below. Table 1 shows that, in the cross section $\eta = 0$ of the tunnel lining, the points $r = R_2$ within the filler are subjected to tensile stresses $\sigma_{\theta\theta}$ and compressive stresses $\sigma_{\eta\eta}$, while at the points on the outer surface of the filler ($r = R_1$), the stresses $\sigma_{\theta\theta}$ and $\sigma_{\eta\eta}$ are tensile. The numerical values of these stresses are only slightly affected by the type of contact between the lining and the rock mass (rigid or sliding). The stresses $\sigma_{\theta\theta}$ at points on the outer surface ($r = R_1$) of the lining filler are approximately twice as large, the stresses $|\sigma_{\eta\eta}|$ are half as large, and the stresses $|\sigma_{rr}|$ are 20 times smaller than the corresponding stresses at points on its inner surface ($r = R_2$).

As follows for θ = const from Tables 1 and 2, in the cross section ($\eta = 0$) of the tunnel, the displacements u_r of the points on the outer surface of the tunnel lining filler and the points on the contact surface of the rock mass are identical. At the same time, the stresses $|\sigma_{rr}|$, $|\sigma_{\theta\theta}|$, and $|\sigma_{\eta\eta}|$ at the outer surface of the filler are significantly higher than those at the corresponding contact surface of the surrounding rock mass.

As shown by the calculations, with increasing distance from the tunnel lining in the vertical direction ($x \to -\infty$, $\eta = 0$), the stresses and displacements in the rock mass decrease and become practically negligible at $|x| = 4 \div 5R_1$.

It follows from Table 3 and **Figures 2–5** that with sliding contact of the lining with the rock mass, the displacements and stresses of the Earth's surface are greater than with rigid contact. Vertical displacements u_x of points (deflections) of the Earth's surface occur upward, and the stresses σ_{yy} and $\sigma_{\eta\eta}$ at these points are tensile. At $y = 0$, displacements u_x and stresses σ_{yy}, $\sigma_{\eta\eta}$ have maximum values and decrease rapidly with increasing $|y|$. Horizontal displacement u_y of points (shifts) of the

Earth's surface at $y < 0$ occurs to the left, at $y > 0$ – to the right ($y = 0$, $u_y = 0$). The maximum ground surface displacements occur at $|y| = 2.6$ m. The displacements u_y of points symmetrically located with respect to the x-axis have identical values.

4 CONCLUSIONS

1. Based on mathematical modeling, an analytical solution has been obtained to investigate the dynamic behavior of a shallow tunnel subjected to stationary transport loading.

2. The tunnel lining, modeled in an elastic half-space, is represented as three rigidly connected circular cylindrical layers with different physical and mechanical properties, including a thick middle layer (filler) and thin outer layers (facing). In the problem formulation, the lining is considered as a circular three-layer shell.

3. The case of a shallow tunnel reinforced with a three-layer steel-concrete lining (comprising a concrete filler and steel facing layers of equal thickness) subjected to a uniformly distributed axisymmetric normal load moving at a constant velocity within a specified interval has been analyzed.

4. Numerical experiments were conducted using a computer program developed by the authors based on the obtained analytical solution to investigate the influence of the type of contact between the lining and the rock mass (rigid or sliding) on the stress–strain state (SSS) of the tunnel lining filler and the surrounding rock mass.

5. It has been established that the type of contact between the tunnel lining and the rock mass significantly affects only the stress–strain state of the rock mass.

6. The displacements and stresses on the ground surface are considerably higher in the case of sliding contact compared to rigid contact.

7. The developed computational software package is intended for use by engineering design organizations involved in tunnel construction.

REFERENCES

1. **Sheng, X.** (2019). A review on modelling ground vibrations generated by underground trains. International Journal of Rail Transportation, 7(4), 241–261. https://doi.org/10.1080/23248378.2019.1591312
2. **Alekseeva, L. A., & Girnis, S. R.** (2009). Research of dynamic behaviour of a trilaminar shell in an elastic space under the action of a moving load [Dinamicheskoe povedenie trekhsloynoy obolochki v uprugom prostranstve pri vozdeystvii podvizhnoy nagruzki]. Mathematical Journal, 9(4), 5–13. https://math.kz/category/mathematical-journal (In Russ.).
3. **Otarbaev, Zh. O.** (2018). Influence of rate of running periodic load in three-layer tunnel lining on the stress–strain state of surrounding massif [Vliyanie skorosti begushchey periodicheskoy nagruzki na reaktsiyu okruzhayushchego massiva v trekhsloynoy obdelke tonnelya]. Bulletin of the National Engineering Academy of the Republic of Kazakhstan, (3), 64–72. https://vestnik.kazgasa.kz/frontend/web/uploads/archive/doc/1608146504_wuFiYT.pdf (In Russ.).
4. **Zhou, S., Zhang, X., Di, H., & He, C.** (2018). Metro train–track–tunnel–soil vertical dynamic interactions: Semi-analytical approach. Vehicle System Dynamics, 56(12), 1945–1968. https://doi.org/10.1080/00423114.2018.1444182
5. **Sheng, X., Jones, C. J. C., & Thompson, D. J.** (2005). Modelling ground vibration from railways using wavenumber finite- and boundary-element methods. Proceedings of the Royal Society A, 461(2059), 2043–2070. https://doi.org/10.1098/rspa.2005.1450
6. **Forrest, J. A., & Hunt, H. E. M.** (2006). A three-dimensional tunnel model for calculation of train-induced ground vibration. Journal of Sound and Vibration, 294(4–5), 678–705. https://doi.org/10.1016/j.jsv.2005.12.032

7. **Hussein, M. F. M., & Hunt, H. E. M.** (2007). A numerical model for calculating vibration from a railway tunnel embedded in a full-space. Journal of Sound and Vibration, 305(3), 401–431. https://doi.org/10.1016/j.jsv.2007.03.068
8. **Zeng, C., Sun, H.-L., Cai, Y.-Q., & Wang, P.** (2014). Analysis of three-dimensional dynamic response of a circular lining tunnel in saturated soil under harmonic loading. Rock and Soil Mechanics, 35(4), 1147–1156. https://doi.org/10.16285/j.rsm.2014.04.026
9. **Gupta, S., Stanus, Y., Lombaert, G., & Degrande, G.** (2009). Influence of tunnel and soil parameters on vibrations from underground railways. Journal of Sound and Vibration, 327(1–2), 70–91. https://doi.org/10.1016/j.jsv.2009.05.029
10. **Dwivedi, J. P., Singh, V. P., Lal, K., & Devi, S.** (2017). Dynamic response of lined circular tunnel in linear viscoelastic medium due to moving ring load. Materials Today: Proceedings, 4(2), 3767–3775. https://doi.org/10.1016/j.matpr.2017.02.273
11. **Di, H., Guo, H., Zhou, S., Wang, B., He, C., & Zhang, X.** (2022). Analytical model for evaluating dynamic response of a tunnel embedded in layered foundation soil with different saturation. Earthquake Engineering and Engineering Vibration, 21(3), 663–681. https://doi.org/10.1007/s11803-022-2120-5
12. **Otarbaev, Zh. O.** (2015). Influence of contact conditions of a two-layer tunnel lining at great depth on its stress–strain state under transport loads [Vliyanie kontaktnykh usloviy dvukhsloynoy obdelki tonnelya glubokogo zalozheniya na ego napryazhenno-deformirovannoe sostoyanie]. Vestnik KazNTU, (2), 274–280. https://vestnik.satbayev.university/index.php/journal/issue/view/21/20 (In Russ.).
13. **Girnis, S., & Bulyga, L.** (2023). Action of moving load on a two-layer shell in elastic medium. In Proceedings of XV International Scientific Conference "INTERAGROMASH 2022" (Lecture Notes in Networks and Systems, Vol. 574, pp. 2301–2311). Springer. https://doi.org/10.1007/978-3-031-21432-5_251
14. **Degrande, G., Clouteau, D., Othman, R., Arnst, M., Chebli, H., Klein, R., Chatterjee, P., & Janssens, B.** (2006). Numerical model for ground-borne vibrations from underground railway traffic based on periodic FE–BE formulation. Journal of Sound and Vibration, 293(3–5), 645–666. https://doi.org/10.1016/j.jsv.2005.12.023
15. **Yang, Y. B., & Hung, H. H.** (2008). Soil vibrations caused by underground moving trains. Journal of Geotechnical and Geoenvironmental Engineering, 134(11), 1633–1644. https://doi.org/10.1061/(ASCE)1090-0241(2008)134:11(1633)
16. **Yang, Y. B., & Li, J.** (2022). 2.5D prediction of soil vibrations due to railway loads using isogeometric analysis with scaled boundary. Engineering Analysis with Boundary Elements, 134, 341–359. https://doi.org/10.1016/j.enganabound.2021.10.012
17. **Zhou, S., He, C., Di, H., Guo, P., & Zhang, X.** (2017). Efficient prediction of train-induced vibrations from tunnel in poroelastic half-space. Engineering Analysis with Boundary Elements, 85, 43–56. https://doi.org/10.1016/j.enganabound.2017.09.013
18. **Yuan, Z., Boström, A., Cai, Y., & Cao, Z.** (2017). Analytical solution for vibrations from tunnel embedded in saturated poroelastic half-space. Journal of Sound and Vibration, 387, 177–193. https://doi.org/10.1016/j.jsv.2016.10.016
19. **Coşkun, I., & Dolmaseven, D.** (2017). Dynamic response of a circular tunnel in an elastic half-space. Journal of Engineering, 2017, 1–12. https://doi.org/10.1155/2017/6145375
20. **Alekseeva, L. A., & Ukrainets, V. N.** (2009). Dynamics of elastic half-space with reinforced cylindrical cavity under moving loads. International Applied Mechanics, 45(9), 75–85. https://doi.org/10.1007/s10778-010-0238-z
21. **Alekseeva, L. A., & Ukrainets, V. N.** (2020). Model of tunnel and shallow pipeline dynamics under traffic loads [Model' dinamiki tonnelya i podzemnogo truboprovoda melkogo zalozheniya]. Bulletin of L. N. Gumilyov ENU. Mathematics. Computer Science. Mechanics, 133(4), 28–39. https://doi.org/10.32523/2616-7182/2020-133-4-28-39 (In Russ.).
22. **Otarbaev, Zh. O.** (2022). Influence of friction during transportation of loads through underground pipelines on stress–strain state of earth surface [Vliyanie treniya pri transportirovke

gruzov po podzemnym truboprovodam]. Bulletin of the Kazakh Leading Academy of Architecture and Civil Engineering, (1), 189–198. https://doi.org/10.51488/1680-080X/2022.1-19 (In Russ.).

23. **Gorshkova, L. V.** (2023). Impact of normal and tangential loads on shallow tunnel. Bulletin of L. N. Gumilyov ENU. Mathematics. Computer Science. Mechanics, 144(3), 12–22. https://doi.org/10.32523/2616-7182/bulmathenu.2023/3.2
24. **Stanevich, V. T.** (2023). Dynamic response of cavities in elastic half-space under moving loads. Bulletin of the Karaganda University. Physics Series, 112(4), 65–75. https://doi.org/10.31489/2023ph4/65-75
25. **Otarbaev, Zh. O.** (2024). Impact of tunnel lining on ground surface reaction under transport loads. Bulletin of the Kazakh Leading Academy of Architecture and Civil Engineering, 3, 79–94. https://doi.org/10.51488/1680-080X/2024.3-06